Charged Diphenylalanine Nanotubes and Controlled Hierarchical Self-Assembly

Minjie Wang,[†] Lingjie Du,[†] Xinglong Wu,[*,†] Shijie Xiong,[†] and Paul K. Chu[*,‡]

[†]National Laboratory of Solid State Microstructures and Department of Physics, Nanjing University, Nanjing 210093, P. R. China, and [‡]Department of Physics and Materials Science, City University of Hong Kong, Tat Chee Avenue, Kowloon, Hong Kong, China

ABSTRACT Hexagonal hierarchical microtubular structures are produced by diphenylalanine self-assembly and the ratio of the relative humidity in the growth chamber to the diphenylalanine concentration (defined as the RH—FF ratio) determines the microtubular morphology. The hexagonal arrangement of the diphenylalanine molecules first induces the hexagonal nanotubes with opposite charges on the two ends, and the dipolar electric field on the nanotubes serves as the driving force. Side-by-side hexagonal aggregation and end-to-end arrangement ensue finally producing a hexagonal hierarchical microtubular structure. Staining experiments and the external electric field-induced parallel arrangement provide evidence of the existence of opposite charges and dipolar electric field. In this self-assembly, the different RH—FF ratios induce different contents of crystalline phases. This leads to different initial nanotube numbers finally yielding different microtubular morphologies. Our calculation based on the dipole model supports the dipole-field mechanism that leads to the different microtubular morphologies.

KEYWORDS: diphenylalanine nanotubes · self-assembly · dipolar electric field · hexagonal hierarchical structures

Hierarchical self-assembly is a natural process that spontaneously organizes molecular units into well-ordered structures and is becoming a popular tool in bottom-up nanotechnology. The inherent biocompatibility and versatile chemical properties of peptide molecules render them excellent building blocks for the formation of various nanostructures *via* hierarchical self-assembly with potential applications in biosensing, catalysis, antibacterial applications, and drug delivery.[1−12] Diphenylalanine (L-Phe-L-Phe, FF), the core recognition motif of the Alzheimer's disease-associated β-amyloid polypeptide, is believed to be one of the simplest building blocks. They can readily self-assemble into various nanostructures such as nano/microtubes (NTs/MTs),[13,14] nanowires,[15−17] microcrystals,[18] and vertically aligned nanoforests.[14] The main products produced from many experiments have a tube-like morphology with diameters ranging from several nanometers to tens of micrometers.

During the NT formation, the FF molecules shed water molecules to form aggregates as inferred by nuclear magnetic resonance.[19] Hence, it is generally agreed that in a common nucleation-driven process, NTs are formed *via* an ordered and hierarchical assembly mechanism. Recent investigations further show that during the formation of nanowires and NTs in solutions, the morphological evolution appears to depend on the amount of free water in the medium.[20] However, in practice, different FF concentrations are usually used. Hence, the amount of water and FF concentration are the two most important parameters dictating the formation of these tube-like structures. To our knowledge, a morphology-controlled study has not been reported and the essential formation mechanism of hierarchical MTs is still unclear. This is hampering further applications of peptide NT/MT structures in many fields.

In this article, we reveal the morphological evolution of hierarchical FF MTs under conditions involving different ratios of relative humidity (RH) in the growth chamber to FF concentrations (RH—FF ratio). Staining experiments and external electric field-induced MT arrangements provide evidence of the existence of opposite charges on the two ends of the MTs. On the basis of the morphologies of the hierarchical FF NTs/MTs, we present a dipolar electric field driven formation mechanism.

RESULTS AND DISCUSSION

Figure 1 panels a—e depict the field emission scanning electron microscopy (FE-SEM) images of five typical morphologies. When the RH—FF ratio (a dimensionless constant C) is less than 0.1, no regular nanostructure can be formed with the exception of a transparent and flat amorphous thin film (data not shown). When C is between 0.1 and 5, different hexagonal NT/MT morphologies emerge. At C = 0.2, small rod-shape nanostructures with an average diameter of ~50 nm appear on the sample

* Address correspondence to hkxlwu@nju.edu.cn, paul.chu@cityu.edu.hk.

Received for review December 9, 2010 and accepted May 18, 2011.

Published online May 18, 2011
10.1021/nn2016524

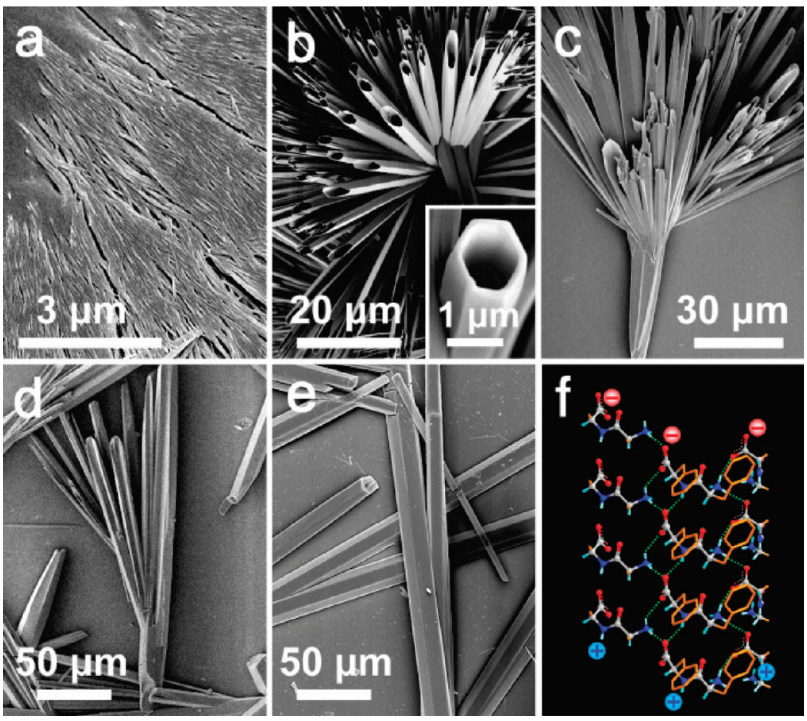

Figure 1. (a−e) FE-SEM images of the hexagonal NTs and MTs formed at difference RH−FF ratios: (a) 0.2, (b) 0.3, (c) 0.5, (d) 0.6−0.9, and (e) larger than 1. The inset in image b shows a representative hexangular MT. (f) The lateral view of the model for a four turn channel. For clarity, FF molecules in the back of each turn are omitted and only the atomic side chains and hydrogen bonds of the four FF molecules facing to us are shown.

surface (Figure 1a). When *C* reaches 0.3, hexagonal MTs several μm in diameter and a few tens of μm long are formed. These MTs exhibit a perfect hexagonal tubular morphology (Figure 1b and its inset) and usually grow in clusters. When *C* is 0.5, many feather-like MT structures with a large head and multilevel clustered tails (Figure 1c) appear. The average diameter of the heads is ~10 μm, which is larger than those in Figure 1b. When *C* is in the range of 0.6−0.9, FF monomers self-assemble into dendritic MTs with larger sizes and fewer tails (Figure 1d). When *C* is more than 1, MTs with an average diameter of 20 μm are formed without divarication (Figure 1e). The above results indicate unequivocally that the RH−FF ratio determines the NT/MT morphology.

According to the size and morphological evolution, it can be inferred that these MT structures are constructed based on the NTs with diameters of 50 nm (Figure 1a). Powder X-ray diffraction (PXRD) patterns are acquired from all the samples and although the PXRD patterns from the samples prepared at low RH−FF ratios show a broad amorphous background, all the diffraction peaks can be indexed to the hexagonal crystalline structure of the FF molecules (space group $P6_1$) as reported previously.[21,22] As the RH−FF ratio increases, the broad background disappears gradually and the crystalline component increases. This increases the initial NT number. Two representative PXRD patterns acquired from the samples prepared at RH−FF ratios of 0.37 and 0.5 are exhibited in Supporting Information, Figure S1a. As described by Gorbitz,[22,23] there is head-to-tail hydrogen bonding between FF molecules in the helix with six FF molecules per turn. As the helix grows, the laminated structure is converted into a channel. The aromatic groups outside the channel stack serve as the glue between different channels. Finally, the structure morphs into a low-density porous supramolecular network. Supporting Information, Figure S1b schematically shows the view from the axial direction of a 50 nm diameter NT, and the magnified image of the area in the solid rectangle is presented in Figure S1c.[21,22] The six FF molecules per turn in the channel give rise to the hexagonal morphology and the NT can be considered as an enlarged area of the hexagonal channel so that the porous NT exhibits a hexagonal appearance.

A lateral view of a channel with four turns is presented in Figure 1f. The top and bottom planes of the channel are oxygen ($-COO^-$) and hydrogen (−NH− and $-NH_3^+$) terminated, respectively. Hence, there are net negative and positive charges on the two ends when a channel is filled with some water molecules *via* hydrogen bonding which forms a dipolar electric field along the channel direction. In the NT structure, the dipolar electric field will be far larger. In a hexagonal helix cell consisting of six FF molecules, the net negative/positive charges of the upper and lower sides are 6e. Based on the cell size,[21,22] we can roughly estimate the maximum positive/negative charges on the two ends of a 50 nm outer and 20 nm inner diameter NT to be ($6e \times 378$) = 2268e (3.63×10^{-16} C). This charge quantity will decrease due to random molecular aggregation caused

by the amorphous component. To specify the effects of dipoles in the aggregation of the FF molecules, a density-functional-theory (DFT) study using the CASTEP package[24] is performed on two stacked FF molecules in the presence of a water molecule.[24] The geometric structure is first optimized using the BFGS minimizer in the CASTEP package, and the spatial distribution of the electron density on the optimized structure is then calculated. The obtained structure and corresponding electron density are shown in Figure 2. It is interesting to note that there is an obvious difference in the electron density between the upper and lower sides of the FF molecules. The DFT calculation shows that the dipole moment of the FF molecule in this stack is 5.84 D. This value is certainly large considering the covalent nature of the molecules. Owing to polarization of water molecules, the presence of water favors the aggregation of FF molecules as illustrated in Figure 2.

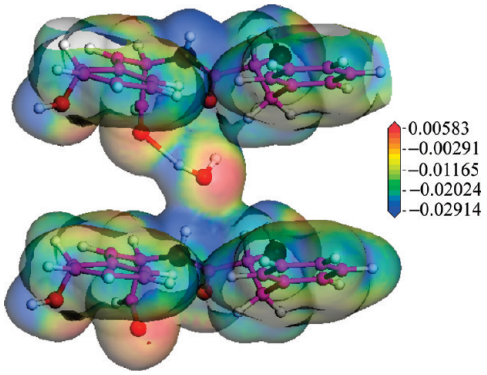

Figure 2. Optimized structure of the stacking of two FF molecules in the presence of a water molecule and the spatial distribution of electron density obtained by DFT calculation. The small white, middle violet, middle red, and big black balls represent H, C, O, and N atoms, respectively. The values of the electron density are the differences with respect to the sum of the electron densities in the corresponding neutral atoms located on the optimized structure in units of electron/Angstrom^3.

To identify the existence of positive/negative charges on the two ends of the NTs, staining experiments are conducted using some positive/negative charged dyes.[23,25] Without charged dyes, the heads and tails of the feather-like MT structures do not show any color difference under optical microscopy (Figure 3a–c). When the samples are mixed with negatively charged Congo Red (Supporting Information, Figure S2a), no tails are stained red (Figure 3d,f), but in the center of the hierarchical MTs, the heads of many MTs are stained red (arrows, Figure 3e and its inset). This suggests that the negatively charged dye molecules only attach to the head side. On the contrary, when positively charged Safranine T is used (Figure S2b), the tails are stained red (Figure 3g,i) and the center part of the MTs is not (Figure 3h). Selective and opposite staining results indicate that the two ends of the NTs/MTs have different charge characteristics thus constructing an intrinsic dipolar electric field. The staining experiments provide direct proof that the tails are negatively charged and the heads are positively charged.

To further indicate the existence of the dipolar electric field, a horizontal external electric field is applied to the slide *via* two Al electrodes parallel to each other. A 30 μL portion of the FF solution is placed on the slide between the two electrodes. This experiment is performed at a RH–FF ratio of 1.11, and optical images are taken after setting for 60 min. When no voltage is applied, the hexagonal tubular structures

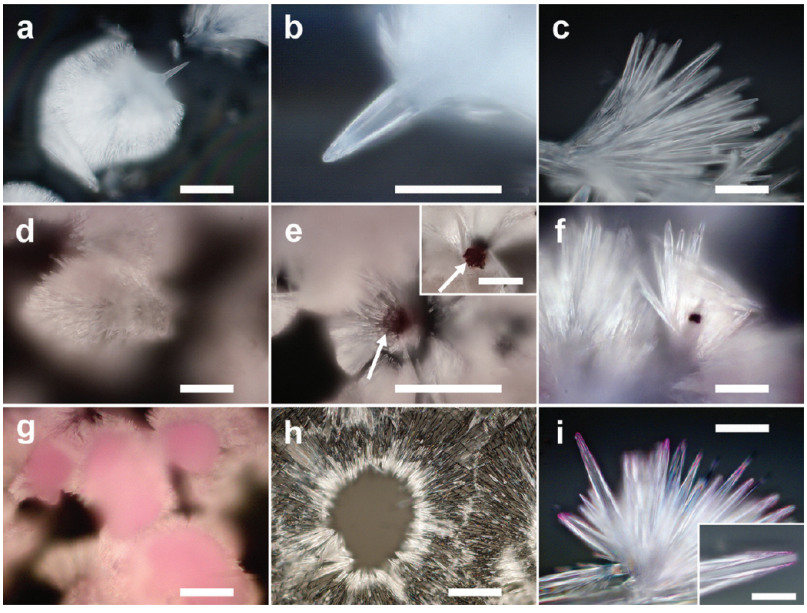

Figure 3. Optical microscope images: (a–c) Pure samples without staining. (d–f) Feather-like structures stained with the negatively charged dye (Congo Red). (g–i) Feather-like structures stained with the positively charged dye (Safranine T). Panels a, d, and g are the complete images (scale bars = 50 μm); panels b, e, and h are images of the heads and the center parts (scale bars = 20 μm); panels c, f, and i are images of the tails (scale bars = 20 μm). Scale bars for insets = 10 μm.

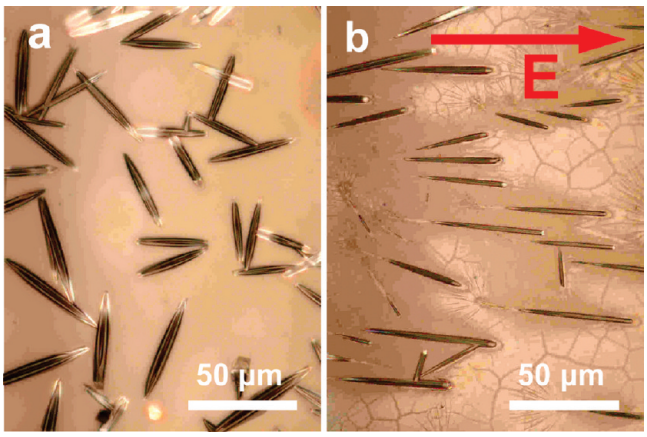

Figure 4. Optical microscope images of the hexagonal tubular structures formed without (a) and with (b) the horizontal external electric field.

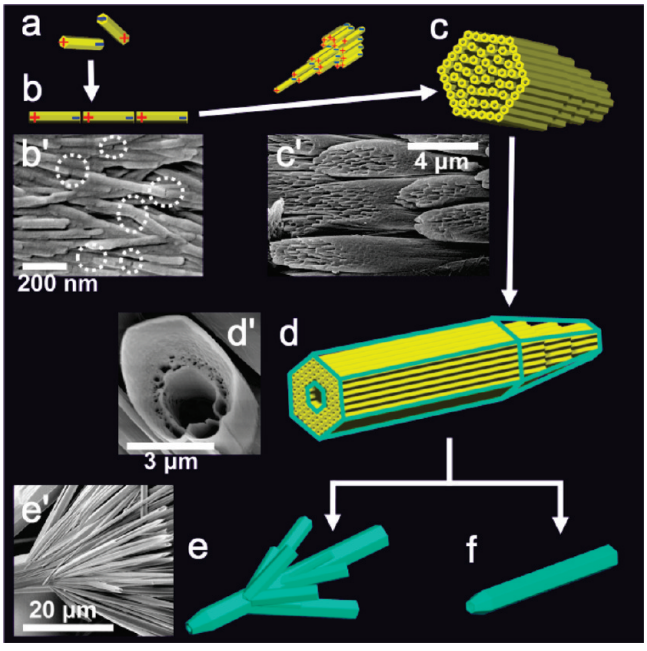

Figure 5. Schematic illustration of the growth process of the NT/MT structures.

with an average diameter of about 20 μm are formed in a disordered fashion (Figure 4a). In comparison, when 150 V is applied between the two electrodes, the tubular structures become more orderly. Most of the tubes are oriented parallel to the external electric field (Figure 4b) and become thinner and longer than those formed without the external electric field. All the slender tubes have a tapered tail pointing to the anode and the head pointing to the cathode. This piece of experimental evidence clearly illustrates that the multilevel MT formation is driven by the dipolar electric field.

Accordingly, a dipolar electric field induced NT/MT formation model is presented in Figure 5. In the initial stage, large quantities of nanostructures with hexagonal columnar morphologies (outer diameters of ~50 nm) are formed due to the presence of water molecules and supersaturation in the solution (Figure 5a). These nanostructures have net positive and negative charges on the opposite ends to produce a dipolar electric field. Since there are many negatively charged centers on the surface sites of the glass slice,[26,27] the positively charged ends will be attracted to the surface negative centers. The dipolar electric field causes aggregation of NTs or end-to-end arrangement due to electrostatic interaction (Figure 5b,b′). As the congeries becomes thicker, the NTs are arranged side-by-side and the aromatic residues on the lateral surface of the NTs stack to stabilize the aggregate. As a result, an intermediate morphology is formed with a large aspect ratio caused by end-to-end connection and an integrated crust arises from the parallel arrangement (Figure 5c,c′). When it grows longer, the parallel arrangement continues and the inner parts aggregate to the crust (Figure 5d,d′). Since the crust is hexagonally arranged, the premorphology morphs into

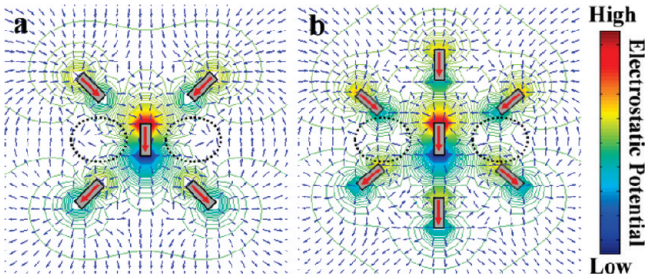

Figure 6. Electric field (blue arrows) and electrostatic potential distributions of (a) low and (b) high dipole densities in the *Y*−*Z* plane. The model prisms (gray rectangles) consist of permanent dipoles (red arrows). The electric field distribution near the central dipole is indicated by the black dashed circles. All the data used to calculate the electrical potential have natural units.

the hexagonal MT. It should be mentioned that because all the NTs are arranged end-to-end and have the same orientation, the MTs also have net positive charges on the heads and negative charges on the tails. To further elucidate the mechanism, the MTs are plotted in cyan (Figure 5d) and reduced to tubes with different charges on two ends and similar aggregation occurs on a larger scale. On the basis of the formation mechanism of the MTs, we believe that the formation of the 50 nm diameter NTs also involves a similar self-assembled process although no growth details are observed.

The RH−FF ratio plays a crucial role in the self-assembly process. Water molecules are needed to form the hexagonal channels and so the availability of water molecules directly impacts the crystal structure. At a low RH−FF ratio, the supply of water to the FF monomers is limited thus resulting in a larger portion of the amorphous phase. The changes in the two phases can be determined from the PXRD patterns (Supporting Information, Figure S1a). Since the amorphous phase does not contribute to the end-to-end and side-by-side arrangements of the NTs, a low RH−FF ratio cannot lead to the formation of the NTs/MTs. As the RH−FF ratio goes up, small amounts of NTs are formed and large MTs appear by the action of the dipolar electric field, but self-assembly is disturbed by the amorphous phase so that some clustered MT structures are formed (Figure 5e). The higher the RH−FF ratio is, the larger is the formed NT number, the bigger is the MT size, and the smaller is the divarication. Finally, when the RH−FF ratio is large enough and the effect of the dipolar electric field is overwhelming, single hexangular MTs without any divarication are produced (Figure 5f). To show the relationship between the resultant MT structure and the RH−FF ratio, the influence of the initial NT number on the MT structure is theoretically evaluated. We use a dipole to represent a NT and a small RH−FF ratio implies that there is a small amount of NTs in the growth system. A larger RH−FF ratio means more formed NTs. Figure 6 plots the electric field and electrostatic potential distributions caused by four and six dipoles in the *Y*−*Z* plane in addition to a central dipole. An increased supply of water molecules during NT formation gives rise to the electric field in the region near the central NT (black dashed circles) gradually aligning parallel to that of the central NT. Hence, the electric field reduces the MT divarication and by increasing the RH−FF ratio, the MTs without divarication can be finally formed. As the patterning of FF assembly can be precisely controlled, the FF hierarchical hexagonal structures have large potential in functional electro-organic hybrid devices.[28] Finally, we would like to point out that a few papers have recently been published to reveal polar dielectric properties of the FF NTs such as piezoelectric effects,[29,30] second harmonic generation,[29] and phase transition with variation of symmetry.[31] These results confirm the main point of our work concerning the electrical dipole structure of these FF NTs.

CONCLUSION

Hexagonal NT-based multilevel FF MT structures are synthesized in a controlled fashion at room temperature using different RH−FF ratios. The crystalline structure formed by hydrogen bonding plays a key role in the FF self-assembly and subsequent formation of various morphologies. It determines the initial hexagonal NT structures with opposite charges on the two ends. The structure then self-assembles into a hierarchical hexagon as a result of the dipolar electric field. The model is corroborated by staining and electric field experiments. The concept of using different RH−FF ratios to alter the morphology of microstructures can be extended to the fabrication of complex functional materials and mesocrystals.

METHODS

Materials. The lyophilized form of FF was purchased from Bachem (Bubendorf, Switzerland), and 1,1,1,3,3,3-hexafluoro-2-propanol (HFP) was purchased from Aladdin (Shanghai, China). Lithium chloride, magnesium chloride, potassium carbonate, magnesium nitrate, sodium bromide, copper chloride, sodium chloride, potassium bromide, and barium chloride were purchased from Nanjing Chemical Reagent Co., Ltd. (Nanjing,

China). Deionized water (18.2 MΩ/cm) produced by a Millipore nanopure water system was used in the experiments.

Preparation of FF Multilevel Hexagonal Structures. The experiments were performed in a cylindrical chamber. The water activity inside the chamber was precisely controlled using different saturated salt solutions covering water activity from zero to one (Supporting Information, Table S1). A slide was washed with pure water and acetone three times, followed by ultraviolet illumination to produce the surface oxygen vacancy centers with one or two electrons. A fixed volume of the saturated salt solution or pure water was put inside the chamber and then incubated overnight to stabilize the water activity. A fresh FF solution was prepared by dissolving the as-received FF in HFP at concentrations from 20 to 300 mg/mL by sonication. To avoid premature aggregation, the FF solution was always prepared fresh. A 30 μL portion of the FF solution was placed on the slide and then kept still for 60 min prior to morphology observation. The experiments were conducted at a constant temperature of 22 °C.

Characterization. The samples were coated with a thin layer of gold before FE-SEM examination (S-4800 CFE-SEM, Hitachi High-technologies Co., Japan). The crystalline structures were analyzed on a Rigaku D/MAX-rA Rotaflex X-ray diffractometer (Rigaku, Co, Japan). Optical microscopy (Nikon Eclipse 80i) was utilized to observe the stained samples and the samples formed under external electric field.

Stain. Two types of dyes, anionic Congo Red and cationic Safranine T, were used without further purification. A 0.3 g/L dye solution was prepared with double distilled water and then the samples on the slice were put into the dye solution slowly. They were kept overnight in dark in a sealed bottle. Afterward, they were taken out and washed thoroughly with double distilled water and then dried. Finally, the slice was inspected by optical microscopy.

Influence of External Electric Field. The experiments were conducted under conditions with a FF concentration of 90 mg/mL at the RH value of 1 at 22 °C. Two Al electrodes parallel to each other and separated by a distance of 5 mm were pressed tightly onto the slide to produce a horizontal electric field. A 30 μL portion of the FF solution was placed on the slide between the two electrodes under an applied voltage of 150 V. In the control experiments, no voltage was applied between the electrodes.

Acknowledgment. This work was supported by National Basic Research Programs of China under Grant Nos. 2007CB936301 and 2011CB922102. Partial support was also from the National and Jiangsu Natural Science Foundations (Nos. BK2008020 and 60976063) as well as Hong Kong Research Grants Council (RGC) General Research Grants (GRF) CityU 112510 and City University of Hong Kong Strategic Research Grant (SRG) No. 7008009.

Supporting Information Available: Water activities (RH) of some saturated salt solutions (Table S1); PXRD patterns of the samples and the top view of the model for the construction of a NT (Figure S1); chemical structures of anionic Congo Red and cationic Safranine T (Figure S2). This material is available free of charge *via* the Internet at http://pubs.acs.org.

REFERENCES AND NOTES

1. Ghadiri, M. R.; Granja, J. R.; Milligan, R. A.; Mcree, D. E.; Khazanovich, N. Self-Assembling Organic Nanotubes Based on a Cyclic Peptide Architecture. *Nature* **1993**, *366*, 324–327.
2. Hartgerink, J. D.; Granja, J. R.; Milligan, R. A.; Ghadiri, M. R. Self-Assembling Peptide Nanotubes. *J. Am. Chem. Soc.* **1996**, *118*, 43–50.
3. Aggeli, A.; Bell, M.; Boden, N.; Keen, J. N.; Knowles, P. F.; McLeish, T. C. B.; Pitkeathly, M.; Radford, S. E. Responsive Gels Formed by the Spontaneous Self-Assembly of Peptides into Polymeric β-Sheet Tapes. *Nature* **1997**, *386*, 259–262.
4. Aggeli, A.; Nyrkova, I. A.; Bell, M.; Harding, R.; Carrick, L.; McLeish, T. C. B.; Semenov, A. N.; Boden, N. Stacking of Beta-Sheet Tapes and Fibre Formation in Solutions of *de Novo* Self-Assembling Peptides. *Proc. Natl. Acad. Sci. U.S.A.* **2001**, *98*, 11857–11862.
5. Fernandez-Lopez, S.; Kim, H. S.; Choi, E. C.; Delgado, M.; Granja, J. R.; Khasanov, A.; Kraehenbuehl, K.; Long, G.; Weinberger, D. A.; Wilcoxen, K. M.; *et al.* Antibacterial Agents Based on the Cyclic D,L-α-Peptide Architecture. *Nature* **2001**, *412*, 452–455.
6. Hartgerink, J. D.; Beniash, E.; Stupp, S. I. Self-Assembly and Mineralization of Peptide-Amphiphile Nanofibers. *Science* **2001**, *294*, 1684–1688.
7. Djalali, R.; Chen, Y.; Matsui, H. Au Nanowire Fabrication from Sequenced Histidine-Rich Peptide. *J. Am. Chem. Soc.* **2002**, *124*, 13660–13661.
8. Mazor, Y.; Gilead, S.; Benhar, I.; Gazit, E. Identification and Characterization of a Novel Molecular-Recognition and Self-Assembly Domain within the Islet Amyloid Polypeptide. *J. Mol. Biol.* **2002**, *322*, 1013–1024.
9. Aggeli, A.; Bell, M.; Boden, N.; Carrick, L. M.; Strong, A. E. Self-Assembling Peptide Polyelectrolyte β-Sheet Complexes Form Nematic Hydrogels. *Angew. Chem., Int. Ed.* **2003**, *42*, 5603–5606.
10. Banerjee, I. A.; Yu, L. T.; Matsui, H. Cu Nanocrystal Growth on Peptide Nanotubes by Biomineralization: Size control of Cu Nanocrystals by Tuning Peptide Conformation. *Proc. Natl. Acad. Sci. U.S.A.* **2003**, *100*, 14678–14682.
11. Madhavaiah, C.; Verma, S. Self-Aggregation of a Reverse Bispeptide Conjugate Derived from the Unstructured Region of the Prion Protein. *Chem. Commun.* **2004**, 638–639.
12. Gao, X. Y.; Djalali, R.; Haboosheh, A.; Samson, J.; Nuraje, N.; Matsui, H. Peptide nanotubes: Simple Separation Using Size-Exclusion Columns and Use as Templates for Fabricating One-Dimensional Single Chains of an Nanoparticles. *Adv. Mater.* **2005**, *17*, 1753–1756.
13. Adler-Abramovich, L.; Aronov, D.; Beker, P.; Yevnin, M.; Stempler, S.; Buzhansky, L.; Rosenman, G.; Gazit, E. Self-Assembled Arrays of Peptide Nanotubes by Vapour Deposition. *Nat. Nanotechnol.* **2009**, *4*, 849–854.
14. Reches, M.; Gazit, E. Controlled Patterning of Aligned Self-Assembled Peptide Nanotubes. *Nat. Nanotechnol.* **2006**, *1*, 195–200.
15. Ryu, J.; Park, C. B. High-Temperature Self-Assembly of Peptides into Vertically Well-Aligned Nanowires by Aniline Vapor. *Adv. Mater.* **2008**, *20*, 3754–3758.
16. Ryu, J.; Park, C. B. High Stability of Self-Assembled Peptide Nanowires against Thermal, Chemical, and Proteolytic Attacks. *Biotechnol. Bioeng.* **2010**, *105*, 221.
17. Ryu, J.; Park, C. B. Solid-Phase Growth of Nanostructures from Amorphous Peptide Thin Film: Effect of Water Activity and Temperature. *Chem. Mater.* **2008**, *20*, 4284–4290.
18. Zhu, P. L.; Yan, X. H.; Su, Y.; Yang, Y.; Li, J. B. Solvent-Induced Structural Transition of Self-Assembled Dipeptide: From Organogels to Microcrystals. *Chem. a Eur. J.* **2010**, *16*, 3176–3183.
19. Carny, O.; Shalev, D. E.; Gazit, E. Fabrication of Coaxial Metal Nanocables Using a Self-Assembled Peptide Nanotube Scaffold. *Nano Lett.* **2006**, *6*, 1594–1597.
20. Kim, J.; Han, T. H.; Kim, Y. I.; Park, J. S.; Choi, J.; Churchill, D. C.; Kim, S. O.; Ihee, H. Role of Water in Directing Diphenylalanine Assembly into Nanotubes and Nanowires. *Adv. Mater.* **2010**, *22*, 583–586.
21. Gorbitz, C. H. The Structure of Nanotubes Formed by Diphenylalanine, the Core Recognition Motif of Alzheimer's β-Amyloid Polypeptide. *Chem. Commun.* **2006**, 2332–2334.
22. Gorbitz, C. H. Nanotube Formation by Hydrophobic Dipeptides. *Chem.—Eur. J.* **2001**, *7*, 5153–5159.
23. Taubert, A.; Palms, D.; Weiss, O.; Piccini, M. T.; Batchelder, D. N. Control of Particle Morphology and Particle Size of Zinc Oxide Precipitated from Aqueous Solution. *Chem. Mater.* **2002**, *14*, 2594–2601.
24. Clark, S. J.; Segall, M. D.; Pickard, C. J.; Hasnip, P. J.; Probert, M. J.; Refson, K.; Payne, M. C. First Principles Methods Using CASTEP. *Zeit. Kryst.* **2005**, *220*, 567–570.

25. Wang, T. P.; Antonietti, M.; Colfen, H. Calcite Mesocrystals: "Morphing" Crystals by a Polyelectrolyte. *Chem.—Eur. J.* **2006**, *12*, 5722–5730.
26. Itoh, C.; Suzuki, T.; Itoh, N. Threshold Energy for Photogeneration of Self-Trapped Excitations in SiO_2. *Phys. Rev. B* **1989**, *41*, 3794–3800.
27. Wu, X. L.; Guo, X. L.; Liu, Z. G.; Siu, G. G.; Jiang, S. S.; Feng, D. Photoluminescence from Optical Waveguiding $LiNbO_3$ Film Formed on Crystalline SiO_2 Substrate by Pulsed Laser Deposition. *Appl. Phys. Lett.* **1996**, *69*, 3963–3965.
28. Adler-Abramovich, L.; Gazit, E. Controlled Patterning of Peptide Nanotubes and Nanospheres Using Inkjet Printing Technology. *J. Pept. Sci.* **2008**, *14*, 217–223.
29. Amdursky, N.; Beker, P.; Shklovsky, J.; Gazit, E.; Rosenman, G. Ferroelectric and Related Phenomena in Biological and Bioinspired Nanostructures. *Ferroelectrics* **2010**, *399*, 107–117.
30. Rosenman, G.; Beker, P.; Koren, I.; Yevnin, M.; Bank, B.; Mishina, E.; Semin, S. Bioinspired Peptide Nanotubes: Deposition Technology, Basic Physics and Nanotechnology Applications. *J. Pept. Sci.* **2011**, *17*, 75–87.
31. Amdursky, N.; Beker, P.; Koren, I.; Bank-Srour, B.; Mishina, E.; Semin, S.; Rasing, T.; Rosenberg, Y.; Barkay, Z.; Gazit, E.; *et al*. Structural Transition in Peptide Nanotubes. *Biomacromolecules* **2011**, *12*, 1349–1354.